J. Fluid Mech. (1999), *vol.* 388, *pp.* 171–195. Printed in the United Kingdom

Miscible porous media displacements in the quarter five-spot configuration. Part 3. Non-monotonic viscosity profiles

By CHRISTIAN PANKIEWITZ† AND ECKART MEIBURG

Department of Aerospace Engineering, University of Southern California, Los Angeles, CA 90089-1191, USA

(Received 13 March 1998 and in revised form 10 December 1998)

The influence of a non-monotonic viscosity–concentration relationship on miscible displacements in porous media is studied for radial source flows and the quarter five-spot configuration. Based on linear stability results, a parametric study is presented that demonstrates the dependence of the dispersion relations on both the Péclet number and the parameters of the viscosity profile. The stability analysis suggests that any displacement can become unstable provided only that the Péclet number is sufficiently high. In contrast to rectilinear flows, for a given end-point viscosity ratio an increase of the maximum viscosity generally has a destabilizing effect on the flow. The physical mechanisms behind this behaviour are examined by inspecting the eigensolutions to the linear stability problem. Nonlinear simulations of quarter five-spot displacements, which for small times correspond to radial source flows, confirm the linear stability results. Surprisingly, displacements characterized by the largest instability growth rates, and consequently by vigorous viscous fingering, lead to the highest breakthrough recoveries, which can even exceed that of a unit mobility ratio flow. It can be concluded that, for non-monotonic viscosity profiles, the interaction of viscous fingers with the base-flow vorticity can result in improved recovery rates.

1. Introduction

Parts 1 and 2 of the present investigation (Chen & Meiburg 1998*a*, *b*) focused on miscible quarter five-spot flows in homogeneous and heterogeneous environments. The evolution of the displacement process was described in detail as a function of the mobility ratio R and the Péclet number Pe, along with the variance and spatial correlation scales of the heterogeneities. Throughout the investigation, a monotonic viscosity–concentration relationship of exponential type was assumed, which may not always represent a close approximation of the miscible fluid combinations used in practical applications. For example, exploratory investigations of enhanced oil recovery processes have employed slugs of alcohol or alcohol mixtures that separate the oil from the water, which is used as the driving fluid, see Latil (1980). These studies demonstrate that it can be advantageous to sandwich a central alcohol slug between layers of a different alcohol that readily absorbs water, so that the main slug remains water-free for longer times. Since different kinds of alcohol are generally

† Permanent address: Lehrstuhl A für Thermodynamik, Technische Universität München, D-85747 Garching, Germany.

miscible with each other, as well as with water and oil, the dependence of the viscosity of these mixtures on the respective concentrations will affect the overall dynamics of the displacement process. As the examples provided by Manickam & Homsy (1993) demonstrate, the relationship between viscosity and concentration of a mixture of alcohols need not be monotonic, but can display a maximum viscosity at intermediate concentration values. Other strategies aim to increase oil recovery by thermal means. In these applications, the non-monotonic dependence of the viscosity of some crude oils on temperature can lead to mobility non-monotonicities, see Farouq Ali (1970). Finally, some enhanced oil recovery schemes have the potential to introduce mobility non-monotonicities by exploiting the dependence of the oil's mobility on the amount of dissolved gas. An example is provided by the so-called 'Water-alternating-gas' schemes, see Christie, Muggeridge & Barley (1991), Blunt & Christie (1991), as well as Latil (1980).

Hence, the stability and nonlinear evolution of miscible displacements for non-monotonic viscosity–concentration relationships poses an interesting and relevant problem, which has been the focus of several recent theoretical and numerical investigations. Hickernell & Yortsos (1986) show that, in the absence of physical dispersion, any rectilinear miscible displacement with a locally unfavourable viscosity profile is unstable. This observation is further confirmed by Chikhliwala, Huang & Yortsos (1988). Bacri, Salin & Yortsos (1992*b*), as well as Bacri *et al.* (1992*a*) extend these investigations and account for dispersion. They demonstrate the existence of a long-wave instability, a most dangerous mode, and a short-wave cutoff. For the step profile associated with time $t = 0$, they identify a single stability parameter. As Manickam & Homsy (1993) point out, this parameter depends only on the end-point derivatives of the viscosity–concentration relationship, rather than on the end-point viscosities themselves. This indicates that non-monotonic profiles can be stable at $t = 0$, even when the end-point viscosities represent an overall unfavourable profile.

Based on a quasi-steady-state approximation, Manickam & Homsy (1993) also investigate the stability behaviour at larger times, when diffusion has resulted in a smooth profile. Overall, a strong influence of the viscosity profile on the dynamics of the flow is demonstrated, which can best be understood in terms of the associated vorticity distributions and streamline patterns displayed by the eigenfunctions. Manickam & Homsy find that displacements characterized by non-monotonic viscosity profiles typically lead to quadrupole structures of the flow field, as opposed to the dipoles observed for monotonic profiles. The convective effects generated by the additional vortical structures are seen to be crucial for the overall stability behaviour. In particular, Manickam & Homsy find that any profile, even if stable initially, will eventually become unstable at a critical time due to the effects of diffusion. This critical time can be seen as an overall measure of the stability of the flow. While the instability growth rates generally increase as the end-point viscosity contrast becomes more unfavourable, the maximum viscosity and the concentration value associated with it strongly influence the stability behaviour as well. Specifically, the results indicate that increasing the maximum viscosity stabilizes displacements with an unfavourable end-point viscosity constrast, while destabilizing those with a favourable one. It is not known how these findings translate to the stability of radial source flows. The stability results for rectilinear flows are confirmed by spectral simulations of the fully nonlinear problem, see Manickam & Homsy (1994). The authors point out important differences to the fingering patterns observed for monotonic profiles, see Tan & Homsy (1988). In particular, for non-monotonic displacements the stable zone of the viscosity profiles acts as a barrier for the forward growth of fingers, which

hence, when viewed in a reference frame moving with the front, tend to propagate backwards. The authors refer to this phenomenon as *reverse fingering*.

Both rectilinear and radially symmetric displacement processes are characterized by base flows that, due to their spatial uniformity, allow us to perform a linear stability analysis. At the same time, these base flows approximate the actual geometries encountered in many applications only to a limited extent. The quarter five-spot configuration represents a case in point. As discussed by Chen & Meiburg (1998*a*), the early stages of this flow are sufficiently similar to a radial displacement that results from linear stability theory apply. During the later stages, however, discrepancies become increasingly noticeable. Potential flow in the quarter five-spot geometry is already subject to a strongly non-radially symmetric strain field. In the presence of a monotonic viscosity-concentration relationship, this strain field and the resulting misalignment of velocity and concentration gradients were seen to immediately result in an elongated dipole-like vortical flow structure, even in the absence of viscous fingering (Chen & Meiburg 1998*a*).

Different viscosity–concentration relationships may result in different vorticity configurations. This is in contrast to radial or rectilinear flows, which, if stable, stay irrotational. In spite of the fact that, in the strict sense of stability theoretical terminology, this rotational flow field is not a 'base flow', we refer to its vorticity as 'base flow vorticity'. Even with the presence of this additional vorticity, locally the stability of the front and the emergence of viscous fingers may still be understood on the basis of stability results for radial or rectilinear displacements, although the effects of shear across the front will have to be taken into account (Rogerson & Meiburg 1993*a*, *b*). However, the global dynamics of the front, and with it the long time evolution of individual fingers and the entire displacement, will be strongly affected by this base-flow vorticity. It is important to realize that the base-flow vorticity is a function of the viscosity profile itself. Hence, when analysing displacements that are neither rectilinear nor radially symmetric, the nature of the viscosity profile is expected not just to affect the fingering process directly, but also indirectly through the base-flow vorticity it establishes. To clarify these interaction mechanisms is the goal of the present investigation.

In § 2 we will apply linear stability theory to radial source flows for non-monotonic viscosity profiles. The results will be interpreted in terms of physical mechanisms. Furthermore, they will aid in validating the direct numerical simulations of quarter five-spot displacements to be discussed in detail in § 3. Section 4 will summarize the findings and present some conclusions.

2. Radial source flow: linear stability analysis

The stability analysis closely follows that of Tan & Homsy (1987) for radial source flows. The dimensionless governing equations expressing the conservation of mass, momentum (Darcy's law), and species in cylindrical coordinates read

$$\frac{\partial}{\partial r}(ru) + \frac{\partial v}{\partial \theta} = 0, \tag{2.1a}$$

$$\frac{\partial p}{\partial r} = -\mu u, \tag{2.1b}$$

$$\frac{\partial p}{\partial \theta} = -\mu r v, \tag{2.1c}$$

$$\frac{\partial c}{\partial t} + u\frac{\partial c}{\partial r} + \frac{v}{r}\frac{\partial c}{\partial \theta} = \frac{1}{Pe}\left[\frac{1}{r}\frac{\partial}{\partial r}\left(r\frac{\partial c}{\partial r}\right) + \frac{1}{r^2}\frac{\partial^2 c}{\partial \theta^2}\right], \tag{2.1d}$$

$$\mu = \mu(c). \tag{2.1e}$$

Here the Péclet number

$$Pe = \frac{Q}{D} \tag{2.2}$$

denotes the relative magnitude of convective and diffusive effects. Both the stability analysis and the direct numerical simulations to be described below account for molecular diffusion only and neglect velocity-dependent dispersion. An overview of the effects of dispersion is provided by Brady & Koch (1988). Yortsos & Zeybek (1988) and Zimmerman & Homsy (1991) investigate the effects of dispersion on the stability and nonlinear evolution of rectilinear miscible displacements in porous media flows. Loggia, Salin & Yortsos (1998) specifically address the influence of dispersion on the stability of non-monotonic mobility profiles in rectilinear displacements. Petitjeans *et al.* (1998) discuss the role of flow-induced dispersion in miscible Hele-Shaw flows, on the basis of experiments and numerical simulations.

In the absence of velocity-dependent dispersion, a self-similar and time-dependent axisymmetric base state can be identified. Sinusoidal perturbations of the radial velocity u' and concentration c',

$$(u', c')(r, \theta, t) = \left(\frac{\Phi}{r}, \Psi\right)(r, t)\mathrm{e}^{\mathrm{i}n\theta}, \tag{2.3}$$

imposed upon this base state give rise to solutions of the resulting stability equations in terms of a similarity variable η,

$$(\Phi, \Psi)(r, t) = (g, h)(\eta) f(t). \tag{2.4}$$

This yields a pair of coupled ordinary differential equations,

$$\frac{\mathrm{d}^2 g}{\mathrm{d}\eta^2} + \left(\frac{1}{\eta} + \frac{1}{\mu_0}\frac{\mathrm{d}\mu}{\mathrm{d}c}\frac{\mathrm{d}c_0}{\mathrm{d}\eta}\right)\frac{\mathrm{d}g}{\mathrm{d}\eta} - \frac{n^2}{\eta^2}g = \frac{n^2}{\eta^2}\frac{1}{\mu_0}\frac{\mathrm{d}\mu}{\mathrm{d}c}h, \tag{2.5a}$$

$$\frac{\mathrm{d}^2 h}{\mathrm{d}\eta^2} + (1 - Pe)\frac{1}{\eta}\frac{\mathrm{d}h}{\mathrm{d}\eta} + \eta\frac{\mathrm{d}h}{\mathrm{d}\eta} - \left(\frac{n^2}{\eta^2} + \sigma\right)h = Pe\frac{1}{\eta}\frac{\mathrm{d}c_0}{\mathrm{d}\eta}g \tag{2.5b}$$

with boundary conditions

$$g, h \to 0 \quad \text{as} \quad \eta \to 0 \quad \text{or} \quad \eta \to \infty, \tag{2.6}$$

where the eigenvalue σ,

$$\sigma = 2t\frac{1}{f}\frac{\mathrm{d}f}{\mathrm{d}t}, \tag{2.7}$$

reflects the existence of an algebraically growing instability. Its growth rate $\sigma/2$ thus is determined by Pe, as well as by the properties of the assumed relationship between viscosity and concentration $\mu = \mu(c)$. The exact nature of this relationship naturally will depend on the particular combination of fluids under consideration. Hence, the present investigation can only attempt to identify some generic features of the displacement process that appear if this relationship is non-monotonic. In order to do this, and to allow comparisons with earlier studies of rectilinear displacements, we employ the same non-monotonic class of viscosity–concentration profiles used by Manickam & Homsy (1993, 1994), which are well suited to represent, for example,

the non-monotonic profiles of alcohol mixtures. They have the form of modified sine functions defined by the expressions

$$\left.\begin{aligned} \mu(c) &= \mu_m \sin(\gamma), \qquad \gamma = \gamma_0(1-\beta) + \gamma_1\beta, \quad \beta = \frac{(1+a)c}{1+ac}, \\ \gamma_0 &= \sin^{-1}\left(\alpha/\mu_m\right), \quad \gamma_1 = \pi - \sin^{-1}\left(1/\mu_m\right), \\ a &= \frac{c_m - \beta_m}{c_m(\beta_m - 1)}, \qquad \beta_m = \frac{\frac{1}{2}\pi - \gamma_0}{\gamma_1 - \gamma_0}, \end{aligned}\right\} \tag{2.8}$$

so that the viscosity-related parameter $R(\mu)$ in the stability equations takes the form

$$R(\mu) = -\frac{1}{\mu}\frac{\mathrm{d}\mu}{\mathrm{d}c} = (\gamma_1 - \gamma_0)\frac{1+a}{(1+ac)^2}\cot(\gamma). \tag{2.9}$$

The coefficients are chosen such that the viscosities of the displacing ($c = 1$) and displaced ($c = 0$) fluid become $\mu(1) = 1$ and $\mu(0) = \alpha$, respectively. The viscosity has a maximum $\mu_m > \alpha$ at $c = c_m$. Note that in the original definition of this profile given by Manickam & Homsy (1993, 1994), the expression for a lacks the factor c_m in the denominator. Figures 1(*a*) and 1(*b*) schematically show the shape of the class of viscosity profile considered, along with the ensuing spatial variation of viscosity for both an unfavourable ($\alpha > 1$) and a favourable ($\alpha < 1$) end-point viscosity contrast. Values of $c_m > 0.5$ correspond to a viscosity maximum located closer to the displacing fluid, which results in a smaller unstable zone in which the viscosity increases in the direction of the base flow. The opposite holds for $c_m < 0.5$.

2.1. *Numerical solution of the stability problem*

The stability equations (2.5) have to be solved numerically for the viscosity–concentration relationship (2.9). In order to minimize stiffness problems for large Pe values, we employ a finite difference approximation to (2.5), thereby obtaining an algebraic eigenvalue problem that can be solved easily with standard methods. In the process, an algebraic mapping is applied that enhances the numerical resolution of the small region around the displacement front. The solution procedure was validated by comparison with the linear stability results of Tan & Homsy (1987) for monotonic profiles. Details can be found in Pankiewitz & Meiburg (1998).

2.2. *Results*

2.2.1. *Dispersion relations*

Dispersion relations are obtained by determining the largest eigenvalue σ as a function of the wavenumber n, for given combinations of Pe and viscosity profile parameters α, μ_m, and c_m. Figure 2 provides representative results for this largest eigenvalue, for $Pe = 400$ and 1200, respectively, and for various values of end-point and maximum viscosities. The location of the viscosity maximum is chosen to be at $c_m = 0.5$ in all cases. Both the wavenumber and the growth rate are scaled with $Pe^{1/2}$, which renders the comparison between results for different Pe-values easier.

As the wavenumber increases from $n = 0$, there are at first no discrete eigenmodes. Below this segment of the curve, only a continuous spectrum of solutions to the stability equations exists. However, this regime usually is very short. At a certain wavenumber, a discrete mode appears above the continuous spectrum, cf. also Manickam & Homsy (1993). Depending on the parameters, the eigenvalue of this mode can become positive and render the flow unstable. We observe a general trend of higher Pe shifting the dispersion relations to higher wavenumbers and larger

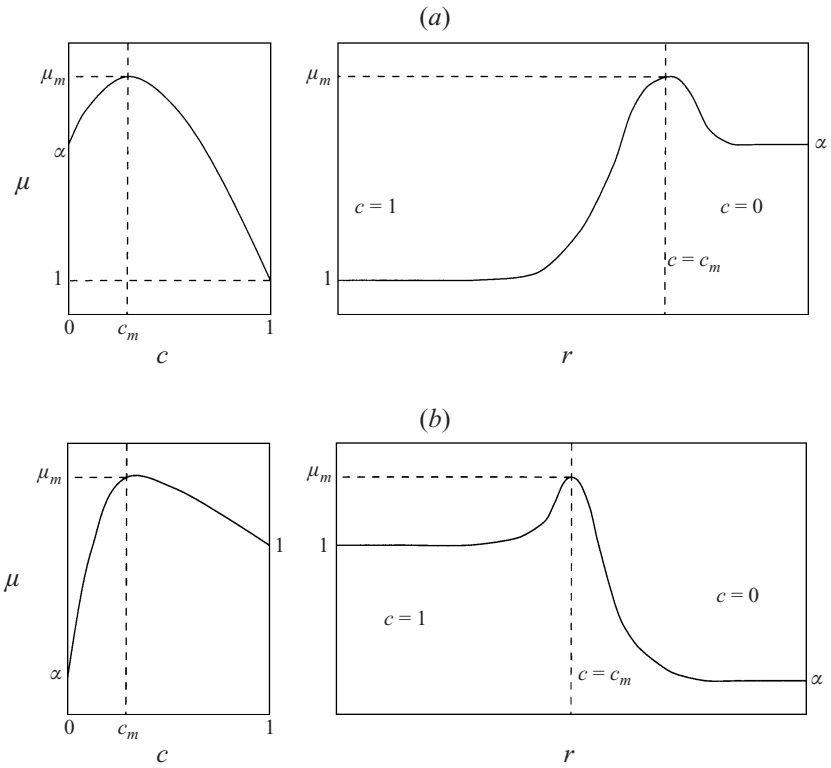

FIGURE 1. Schematic of the non-monotonic viscosity profile (left) and the resulting spactial variation of viscosity for a diffused concentration profile (right) for (*a*) $\alpha > 1$ and (*b*) $\alpha < 1$, cf. Manickam & Homsy (1994).

growth rates. Several properties of the dispersion relationships depicted in figure 2 can be interpreted on the basis of results obtained by Yortsos (1987). He showed that, for large values of *Pe*, the problem of a radial miscible displacement can be transformed into an equivalent rectilinear one, for a suitably modified base state. Consequently, many features of the dispersion relationships for radial flows can be derived in a straightforward fashion from the more extensively studied rectilinear case. Yortsos exploited this fact to provide asymptotic results in the limit of small scaled wavenumbers n_1. From these, it follows directly that the maximum eigenvalue for $n_1 = 0$ is exactly -2, in agreement with figure 2. Furthermore, the slope of σ vs. n at $n = 0$ is predicted to be $(\alpha - 1)/(\alpha + 1)$, and not to depend on *Pe* or μ_m. Again, these features are confirmed by the above figures.

As a general point, our numerical results for a large variety of parameter combinations suggest that for any viscosity profile a critical value Pe_c can be identified, above which there exists an unstable mode. This observation is remarkable, as it implies that even for favourable end-point viscosity contrasts, the unstable zone between the viscosity maximum and the displacing fluid has the ability to trigger an overall instability, provided only that *Pe* is sufficiently large. This indicates that for non-monotonic radial flows unconditionally stable viscosity profiles do not exist. This finding appears to have a corresponding counterpart in rectilinear flows, which were investigated theoretically in the limit of negligible diffusion and dispersion by Hickernell & Yortsos (1986). Based on an analysis of the infinite set of eigenvalues, these authors

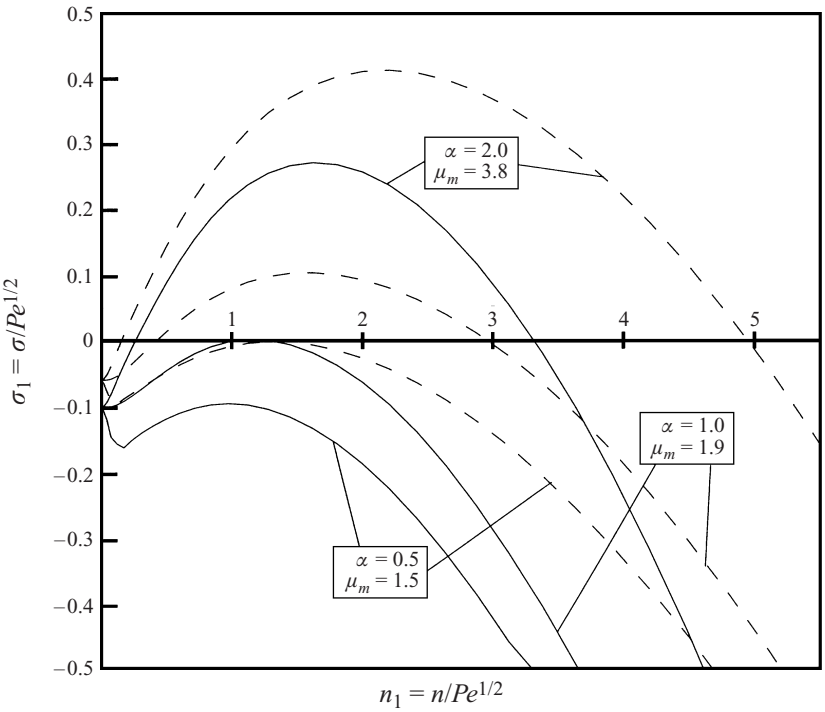

FIGURE 2. Dispersion relations of the largest eigenvalue σ scaled by $Pe^{1/2}$ versus $n_1 = n/Pe^{1/2}$ for $c_m = 0.5$ with α and μ_m as parameters. The solid lines correspond to $Pe = 400$ whereas the dashed lines correspond to $Pe = 1200$.

demonstrate that any rectilinear miscible displacement with a locally unfavourable viscosity profile is unstable in the absence of diffusion and dispersion. In addition, the results by Manickam & Homsy (1993) for rectilinear displacements show that, even in the presence of diffusion, all rectilinear displacements with non-monotonic viscosity–concentration relationships eventually become unstable for sufficiently long times, even if they are initially stable. Loggia *et al.* (1998) extend these results to displacements involving dispersion, and they establish the connection with the classical case studied by Hickernell & Yortsos (1986). Physically, the existence of a critical Péclet number results from differences in the way the respective length scales of the base flow and the most dangerous perturbation depend on Pe. While the radial extent of the base concentration profile scales with $Pe^{-1/2}$, the wavelength of the most dangerous mode exhibits a scaling in the range $Pe^{-(0.7-0.8)}$, see below. This indicates a diminishing influence of the azimuthal diffusion with increasing Pe-values, so that the scale of the most dangerous perturbation decreases relative to the size of the unstable region of the viscosity profile. Hence, above a certain critical value, the evolution of the perturbation mode will be dominated by this unstable region, and the perturbation will grow.

All dispersion relations are found to have one mode for which the growth constant reaches a maximum σ_m, at a corresponding wavenumber n_m or scaled wavenumber $n_{1,m}$, respectively. The σ vs. n plots furthermore always show both a long-wave and a short-wave cutoff. Of particular interest is the short-wave cutoff at wavenumber n_c, as it determines the shortest length scale on which instabilities can develop.

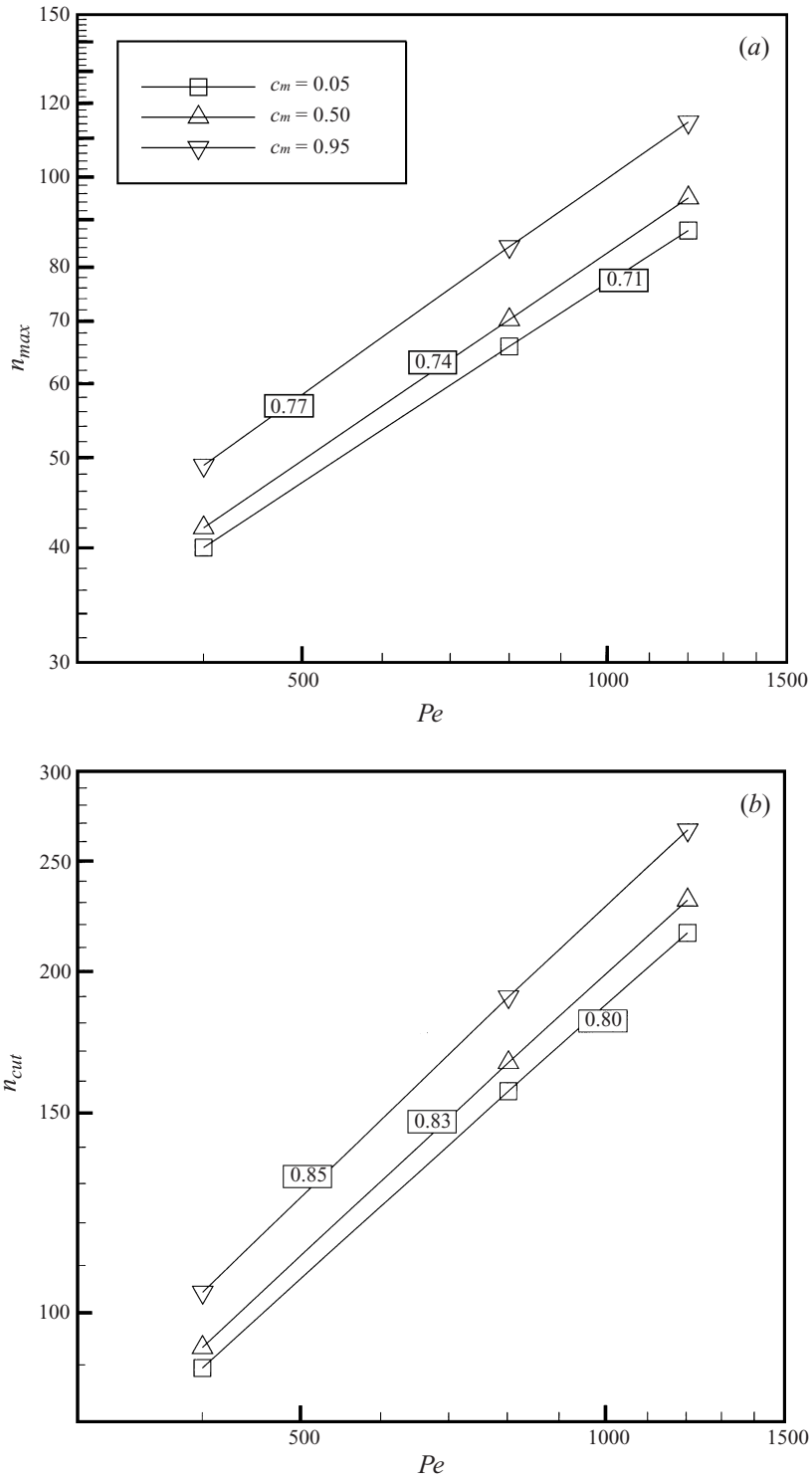

FIGURE 3. (*a*) Wavenumber of the most dangerous mode and (*b*) short-wave cutoff wavenumber versus Péclet number with c_m as a parameter, $\alpha = 5.0$, $\mu_m = 10.0$. The numbers in the boxes show the slope $\Delta \log(n_{max})/\Delta \log(Pe)$ and $\Delta \log(n_{cut})/\Delta \log(Pe)$.

2.2.2. *Parametric study*

In the following, we will summarize the results of systematic parameter variations, in order to elucidate their influence on the overall stability features of the viscosity profiles, as quantified by the most dangerous mode along with the short-wave cutoff.

For both globally favourable and unfavourable viscosity contrasts, we find the growth rates at constant values of c_m to increase monotonically with increasing maximum viscosity μ_m. For $\alpha < 1$, this corresponds to the declining critical times observed for rectilinear displacements at $\alpha = 0.2$ by Manickam & Homsy (1993). For $\alpha > 1$, however, this is in marked contrast to rectilinear displacements with $\alpha = 5$, which were stabilized (in terms of the critical time) by larger values of μ_m. This observation raises the question as to whether a non-monotonic viscosity profile can increase the efficiency of the overall displacement process, as it did for rectilinear flows. This point will be addressed in § 3 by means of detailed nonlinear simulations.

For globally stable viscosity contrasts, the location c_m of the viscosity maximum has a distinct influence on the growth rate, as both large and small values of c_m are seen to reduce σ_m. While a small value of c_m results in a milder unfavourable gradient of the viscosity profile, large values lead to a progressively narrower unstable zone. The overall stability properties are determined by a combination of these two features, so that maximum growth rates are observed for an intermediate value of c_m. For globally unstable viscosity contrasts, on the other hand, there is no maximum of σ_m at intermediate c_m. The growth constants increase with increasing c_m, even though the unstable zone gets very small, indicating that the stronger unfavourable gradients in the viscosity profile become the dominant destabilizing factor.

For $\alpha < 1$, i.e. globally favourable mobility ratios, the most dangerous mode tends to have a shorter wavelength for higher viscosity maxima, and generally also for higher c_m. The cutoff wavenumber, on the other hand, is lower for both narrow and wide unstable zones, and it has a *maximum* in between. The location of this maximum shifts to higher values for increasing maximum viscosity values. This indicates that, for the present globally favourable mobility contrast, the preferred mode and the diffusive short-wave cutoff are influenced differently by the parameters of the viscosity profile, so that we cannot find a simple relation between n_m and n_c. This is in contrast to unfavourable end-point viscosity ratios, for which the cutoff wavenumber is clearly correlated to n_m. We find an algebraic dependence of n_c on n_m,

$$n_c = n_m^{\kappa}, \tag{2.10}$$

where κ varies slightly with c_m and ranges between about 1.18 for $c_m = 0.05$ and 1.20 for $c_m = 0.95$. Interestingly, Tan & Homsy (1987) observe the same behaviour for radial displacements with monotonic exponential viscosity profiles, with a value for κ of approximately 1.2. The range of 1.18–1.20 is also fairly close to the value of 1.125 predicted by Yortsos (1987) in the limit of $Pe \gg 1$ for the equivalent rectilinear problem, based on asymptotic expansions that assume $n/Pe^{1/2}$ to be small.

For large unfavourable viscosity contrasts, we observe a decreasing influence of μ_m/α on σ_m with increasing α. This can be explained by the strongly growing unfavourable gradient in the viscosity profile at $c = 1$. Equations (2.8) and (2.9) show that, for $\alpha \to \infty$ but μ_m/α bounded, $\gamma_1 \to \pi$ and thus $\cot(\gamma_1) \to \infty$, whereas $\cot(\gamma_0)$ remains bounded. Consequently, $R(\mu)$ becomes exeessively large in the unstable zone independent of α/μ_m, if only α is high enough.

Figures 3(*a*) and 3(*b*) demonstrate the scaling of the wavenumber of the most dangerous mode as well as the cutoff wavenumber with Pe. As already observed by

Tan & Homsy (1987) for the exponential viscosity profile, the two wavenumbers scale with different powers of Pe. These powers both increase with c_m. Interestingly, the results for $c_m = 0.05$, $n_m \propto Pe^{0.71}$ and $n_c \propto Pe^{0.80}$, agree closely with the values found by Tan & Homsy. This may be attributed to the fact that for $c_m = 0.05$ the unstable zone has essentially the same width as for the exponential viscosity–concentration relationship. The scaling of n_m and n_c with Pe thus seems to be independent of the detailed shape of the viscosity profile and only to be a function of the width of the unstable zone. The exponents given in figure 3 are also fairly close to the values of $\frac{2}{3}$ and $\frac{3}{4}$ obtained by Yortsos (1987) on the basis on the equivalent rectilinear problem. This is particularly interesting since his results are based on asymptotic expansions that assume $n/Pe^{1/2}$ to be small, whereas the data presented in figure 3 lie outside this range. This indicates that the scaling results of Yortsos are valid beyond this asymptotic regime. More detailed quantitative results can be found in Pankiewitz & Meiburg (1998).

2.2.3. *Physical mechanisms*

For an analysis of the governing physical mechanisms, detailed information about the spatial distribution of the concentration and velocity perturbations is required. Such information can be obtained in a straightforward fashion from the eigensolutions of the stability problem. For $\alpha = 0.2$ and $\mu_m = 2.0$, figures 4(*a*)–4(*c*) depict the concentration eigenfunction of the most dangerous modes for three locations of the viscosity maximum at $c_m = 0.05$, $c_m = 0.50$ and $c_m = 0.95$, respectively. Also shown is the location of the mean interface at $\eta = Pe^{1/2}$, where the concentration becomes $c = 0.5$. The maximum perturbations of the concentration are observed at the mean interface for $c_m = 0.05$, and they drift towards the side of the displacing fluid for higher c_m. This indicates that in the unstable case, viscous fingers will grow inward from the mean interface location. Thus we expect reverse fingering to be a feature of radial displacements with nonomonotonic viscosity profiles, corresponding to the findings for rectilinear displacements by Manickam & Homsy (1994).

Using the eigenfunction of the radial velocity component, along with the azimuthal velocity component as determined from the continuity equation, we obtain for the eigenfunction of the vorticity perturbation

$$\omega' = \left(\frac{1}{n} \frac{\partial^2 \Phi}{\partial r^2} + \frac{1}{n} \frac{1}{r} \frac{\partial \Phi}{\partial r} - n \frac{1}{r^2} \Phi \right) \mathrm{i} e^{\mathrm{i}n\theta} . \tag{2.11}$$

Figure 5 displays the result for the second of the viscosity profiles discussed above, $c_m = 0.50$. In addition, a curve is included that shows the spatial variation of the viscosity, so that the structure of the perturbations can be related to the shape of the viscosity profile. The observed eigenmode has two concentric rings of vortical regions of alternate signs. These rings touch each other exactly at the location of the viscosity maximum. By combining the momentum equations with an alternative expression for the vorticity perturbation

$$\omega' = \frac{1}{\mu_0} \frac{\mathrm{d}\mu}{\mathrm{d}c} \left(\frac{1}{r^2} \frac{\partial c'}{\partial \theta} - v' \frac{\partial c}{\partial r} \right), \tag{2.12}$$

it becomes clear that this vortical structure is a consequence of the non-monotonicity in the viscosity distribution. Consequently, the explanation of the stability mechanism for rectilinear displacements as suggested by Manickam & Homsy (1993) promises to be of relevance for the radial flow as well. The inner vortices are expected to redistribute the viscosity in a way that increases mobility in regions where the velocity

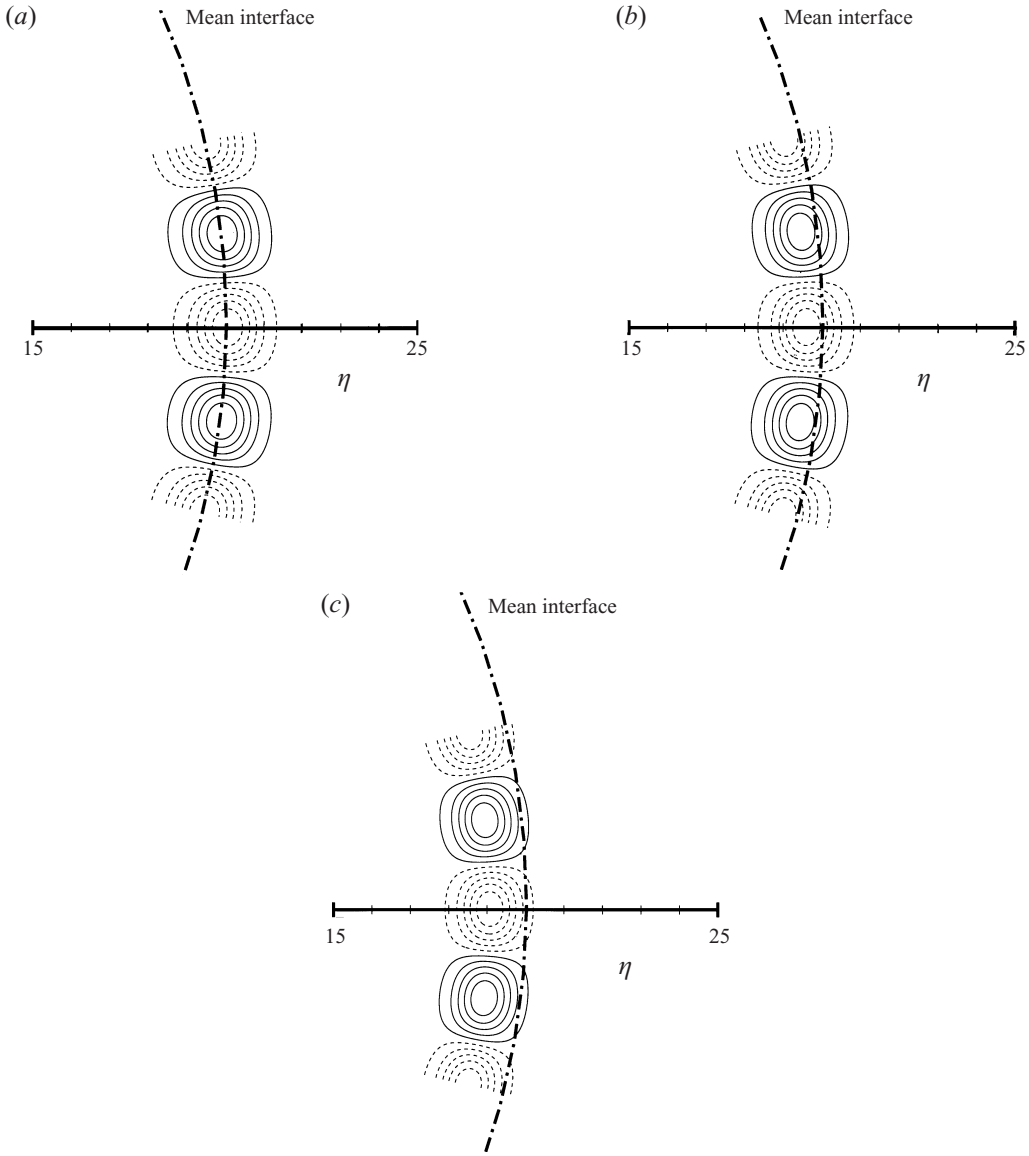

FIGURE 4. Eigenfunction of the concentration perturbation for the least stable mode. The viscosity profile with $\alpha = 0.2$, $\mu_m = 2.0$ and at $Pe = 400$: (*a*) $c_m = 0.05$ (yields $n_m = 25$, $\sigma_m = -0.43$); (*b*) $c_m = 0.50$ (yields $n_m = 25$, $\sigma_m = 0.15$); (*c*) $c_m = 0.95$ (yields $n_m = 26$, $\sigma_m = -1.2$). Positive perturbations are plotted with solid lines, negative perturbations with dashed lines. The location of the mean interface is also shown.

perturbations have the same direction as the base flow, and that decreases mobility where perturbation and base flow have opposite directions, so that disturbances are amplified. The outer vortices transport low-viscosity fluid in regions of high viscosity against the base flow and vice versa, playing a stablilizing role. Manickam & Homsy then argue that the flow will be unstable if the destabilizing vortices are stronger than the stabilizing ones, and stable otherwise. However, inspection of figure 5 indicates that this explanation might not be fully sufficient for the radial case. We find the

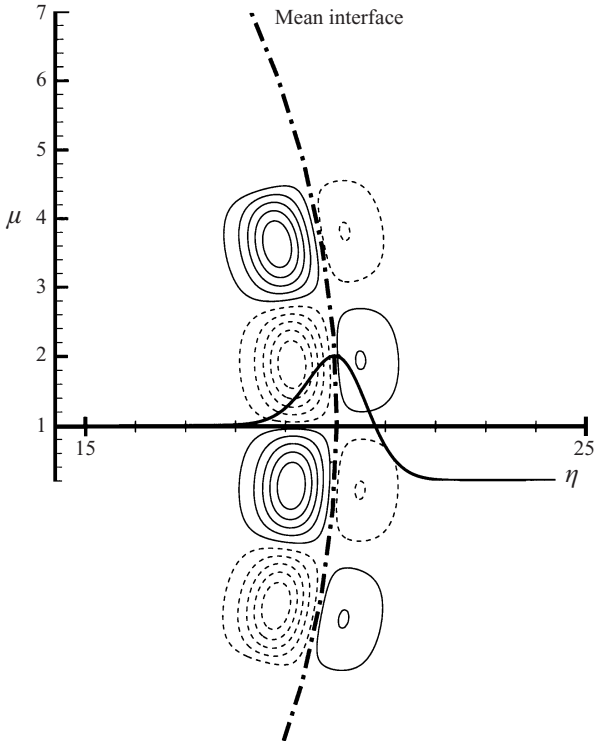

FIGURE 5. Eigenfunction of the perturbation voriticity for the most unstable mode. The viscosity profile with $\alpha = 0.2$, $\mu_m = 2.0$ and $c_m = 0.50$ at $Pe = 400$ yields $n_m = 25$ and $\sigma_m = 0.15$. Positive perturbations are plotted with solid lines, negative perturbations with dashed lines. The spatial variation of the viscosity and the location of the mean interfave are also shown.

inner ring of vortices to be considerably stronger than the outer one. Nevertheless, the displacement is almost neutrally stable with $\sigma_m = 0.15$.

In trying to understand the physical mechanisms, we found the perturbation streamfunction ψ' to be a more meaningful variable to analyse than the vorticity. In cylindrical coordinates, it can be obtained from the radial perturbation velocity by using the definition

$$u' = \frac{1}{r}\frac{\partial \psi'}{\partial \theta}, \tag{2.13}$$

which yields

$$\psi' = -\frac{1}{n}\Phi \mathrm{i} \mathrm{e}^{\mathrm{i}n\theta} + \psi'_0 \tag{2.14}$$

with an integration constant ψ'_0. The perturbation streamfunctions for the three examples mentioned above are presented in figure 6. It is instructive first to analyse the case of $c_m = 0.95$, figure 6(a). This displacement is stable with a maximum eigenvalue $\sigma_m = -1.2$. But we do not find the outer ring of recirculating fluid to which we attributed the stabilizing effect. This, in turn, means that the inner ring must have taken the stabilizing role. This somewhat surprising result can be explained as follows. The vorticity field always has to show two rows of vorticity patches of opposite signs on opposite sides of the viscosity maximum. The corresponding perturbation streamlines, on the other hand, may organize into one or two rows of recirculating fluid. The former is the case in figure 6(a). The recirculating fluid regions

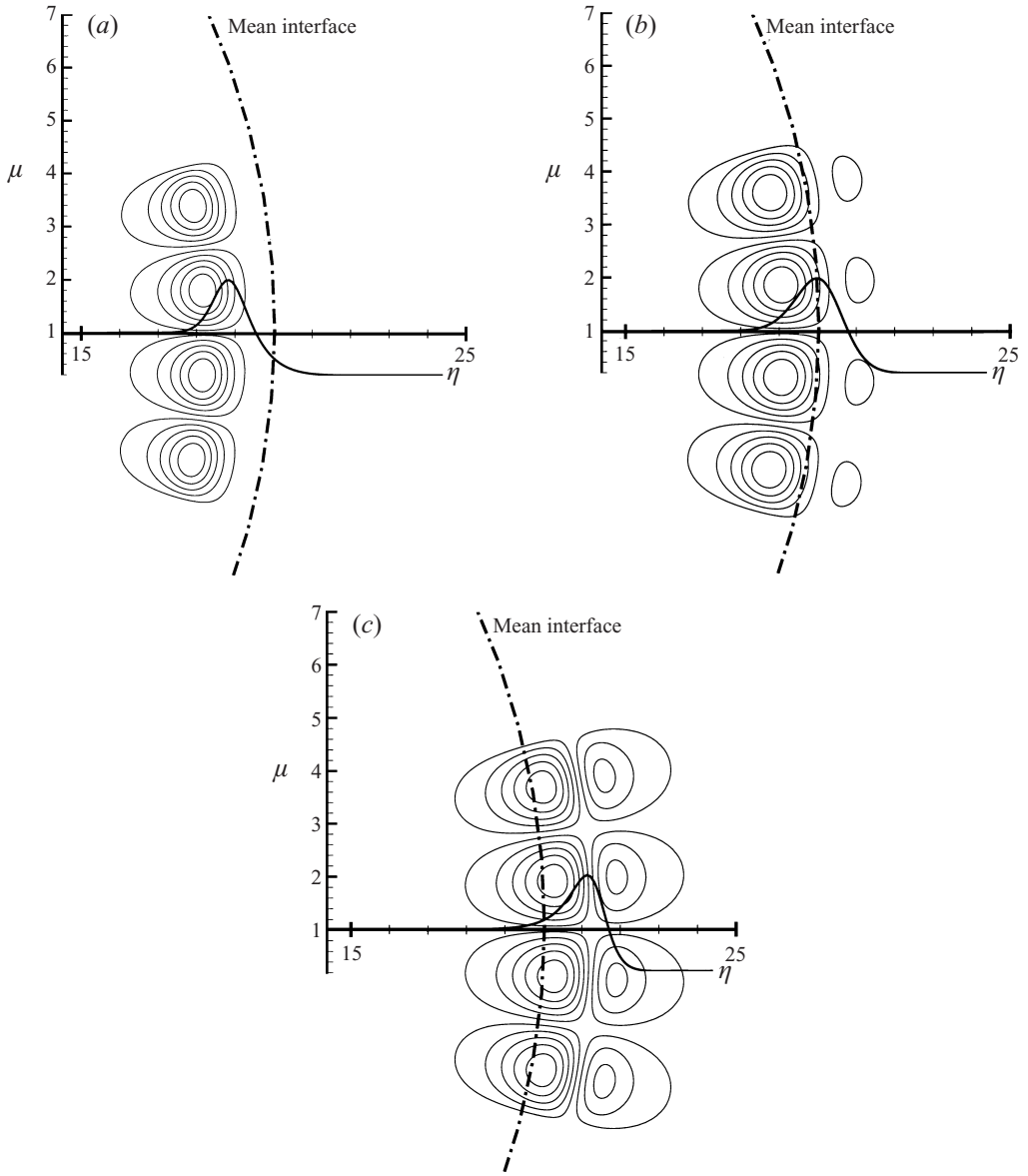

FIGURE 6. Eigenfunction of the perturbation streamfunction for the least stable mode. The viscosity profile with $\alpha = 0.2$, $\mu_m = 2.0$ at $Pe = 400$: (*a*) $c_m = 0.95$ (yields $n_m = 26$ and $\sigma_m = -1.2$); (*b*) $c_m = 0.5$ (yields $n_m = 25$ and $\sigma_m = 0.15$); (*c*) $c_m = 0.05$ (yields $n_m = 25$ and $\sigma_m = -0.43$). The spatial variation of the viscosity and the location of the mean interface are also shown.

in the single ring furthermore extend beyond the base-state location of the viscosity maximum. Thus this flow field structure transports high-viscosity fluid into regions that originally were occupied by low-viscosity fluid due to the globally favourable viscosity ratio, and vice versa. This clearly must stabilize the flow.

For $c_m = 0.50$, a weak outer ring of recirculating fluid becomes noticeable in the perturbation streamfunction, figure 6(*b*). However, it is not yet strong enough to stabilize the flow. Only as c_m further decreases to 0.05 does the outer ring gain enough strength to render the displacement stable, figure 6(*c*). The recirculating fluid

rings are now located on opposite sides of the viscosity maximum. Only under these circumstances does the original argument regarding their stabilizing and destabilizing roles, respectively, apply. If the recirculating fluid regions extend beyond the viscosity maximum, it is more instructive to analyse the streamfunction contours, as opposed to the vorticity contours. We conclude that the strength of the recirculation regions, their location, and their interaction with the gradients in the viscosity profile all influence the stability of the radial flow. This explains the non-monotonic dependence of the growth rate on the location of the viscosity maximum observed earlier.

For unfavourable end-point viscosity ratios we found that usually only the inner recirculating fluid region exists, which at most extends a small distance beyond the viscosity maximum, thereby stabilizing the displacement. More detailed information for different values of c_m can be found in Pankiewitz & Meiburg (1998).

It remains to explain the increase of the growth rates with μ_m even for unfavourable end-point viscosity ratios in radial displacements, which contrasts with earlier findings for rectilinear flows. In (2.12), the first term in the parentheses generally dominates over the second one. Hence it is clear that the maximum vorticity decreases with $1/r^2$ in the radial direction. This will favour the destabilizing inner recirculating fluid regions over the stabilizing outer ones, a mechanism that is absent in rectilinear flows.

3. Direct numerical simulations of quarter five-spot flows

It was straightforward to adapt the original code (Meiburg & Chen 1998) employed for monotonic viscosity profiles (Chen & Meiburg 1998*a*, *b*) to the present non-monotonic case. However, the locally very high absolute values of R for our class of non-monotonic profiles forced us to consider relatively moderate end-point viscosity contrasts, in order to avoid having to use excessively fine grids and small time steps. We furthermore enlarged the core size of the Gaussian source term (Meiburg & Chen 1998) from 0.05 to 0.1. Table 1 gives a summary of the physical and numerical parameters of our calculations. The focus is on the two Pe-values of 200 and 800, while α was held at 2.0 for all simulations. The influence of the degree of non-monotonicity in the viscosity profile on the fingering and the overall efficiency of the displacement was evaluated by employing two different maximum viscosities for $Pe = 800$. The effect of a change in the location of the viscosity maximum was investigated for both Péclet numbers. As in most of the calculations for the homogeneous monotonic case (Chen & Meiburg 1998*a*), the base-state solution at $t = 0.02$ was taken as the initial condition. The nonlinear computational code was validated by comparison with linear stability results. For details, we refer to Pankiewitz & Meiburg (1998).

3.1. $Pe = 200$

Both of the parameter combinations for $Pe = 200$ result in a flow that is dominated by a quadrupole structure in the vorticity distribution. Detailed time traces of the flow evolution can be found in Pankiewitz & Meiburg (1998). At these low Pe-values, this flow feature is merely a consequence of the overall flow geometry, and it does not reflect the growth of similarly structured eigenfunctions associated with linearly unstable perturbations. Nevertheless, the quadrupole structure contrasts with the dipole-like features observed for the monotonic case. While the inner vortex pair accelerates the flow along the diagonal, the outer pair counters this trend and tends to generate a backflow. For $c_m = 0.63$, this trend is more pronounced than for $c_m = 0.37$, and it delays the breakthrough considerably.

Viscosity profile	Pe	α	μ_m	c_m	σ_m	N	δt	Sweep efficiency in %
Non-monotonic	200	2.0	4.0	0.37	2.51	257	5.0×10^{-5}	72.54
Non-monotonic	200	2.0	4.0	0.63	2.63	257	2.0×10^{-5}	> 72.88
Non-monotonic	800	2.0	3.0	0.37	7.22	513	2.0×10^{-5}	69.64
Non-monotonic	800	2.0	4.0	0.25	10.0	513	2.0×10^{-5}	69.55
Non-monotonic	800	2.0	4.0	0.37	10.5	513	2.0×10^{-5}	73.69
Constant	∞	1.0						71.78
Exponential	800	2.0			2.24			63.15
Exponential	800	0.5						94.56

TABLE 1. Parameters, growth rates predicted by linear stabilty theory and breakthrough recovery of the quarter five-spot simulations. N is the number of grid-points in one direction, δt is the time-step employed. For comparisons the value for the unit mobility ratio flow is provided, as are those for exponential viscosity profiles with end-point ratios of 2 and 0.5, respectively.

3.2. $Pe = 800$

Linear stability analysis predicts positive growth rates for all of the parameter combinations discussed in this section. However, vigorous fingering is not always observed. For viscous fingers to become prominent, their growth will have to be sufficiently fast to dominate over the base-flow vorticity, and to reach significant amplitudes before breakthrough occurs. The simulation for $Pe = 800$, $\alpha = 2.0$, $\mu_m = 3.0$ and $c_m = 0.37$, shown in figure 7, illustrates these facts. Up until $t = 0.35$ it evolves similarly to the lower-Pe cases. At $t = 0.40$, however, a new vortical structure can be found on the diagonal, shown in detail in figure 8. There, between the original inner vortices of the basic flow, we find two small vortices which tend to impede the flow along the diagonal. This is reflected by a small bump in the concentration contours, at the inside of the front and pointing towards the source (figure 7). The appearance of this vortical structure indicates the onset of viscous fingering. However, as breakthrough happens shortly thereafter, the emerging fingers do not have time to reach large amplitudes.

The two cases of $Pe = 800$, $\alpha = 2.0$, $\mu_m = 4.0$, and $c_m = 0.25$ and 0.37, respectively, represent situations in which fingers grow to significant amplitudes, see figures 9 and 10. The concentration field develops a slight waviness around $t = 0.20$, which is triggered by the evolution of vortex pairs. These structures grow in time, especially near the diagonal. However, while the outer concentration contours are only marginally affected, large distortions emerge on the side of the displacing fluid. This is a manifestation of reverse fingering, which was anticipated on the basis of our linear stability results, and which is known to dominate rectilinear displacements for non-monotonic viscosity profiles (Manickam & Homsy 1994). Linear stability theory had furthermore shown that the development of fingers is related to the existence of two rings of vortices of opposite sign, one ring on each side of the viscosity maximum. The representative detail of the vorticity field shown by figure 11 confirms this structure, which resides on top of the quadrupole structure of the base-flow vorticity. When the vortical regions associated with fingering are of the opposite sign to the outer base-flow vortex, they become clearly visible. We have marked two of these vortices A and B. Otherwise they merge with the base-flow vortex and extend it inward, marked C. Nevertheless, for the present parameter combination the outer vortices of the quadrupole structure are fairly weak, as was to be expected from linear stability theory.

In the above flows, the spatial phase of the evolving vorticity and streamfunction perturbations plays a crucial role. It takes a value that causes the perturbations to

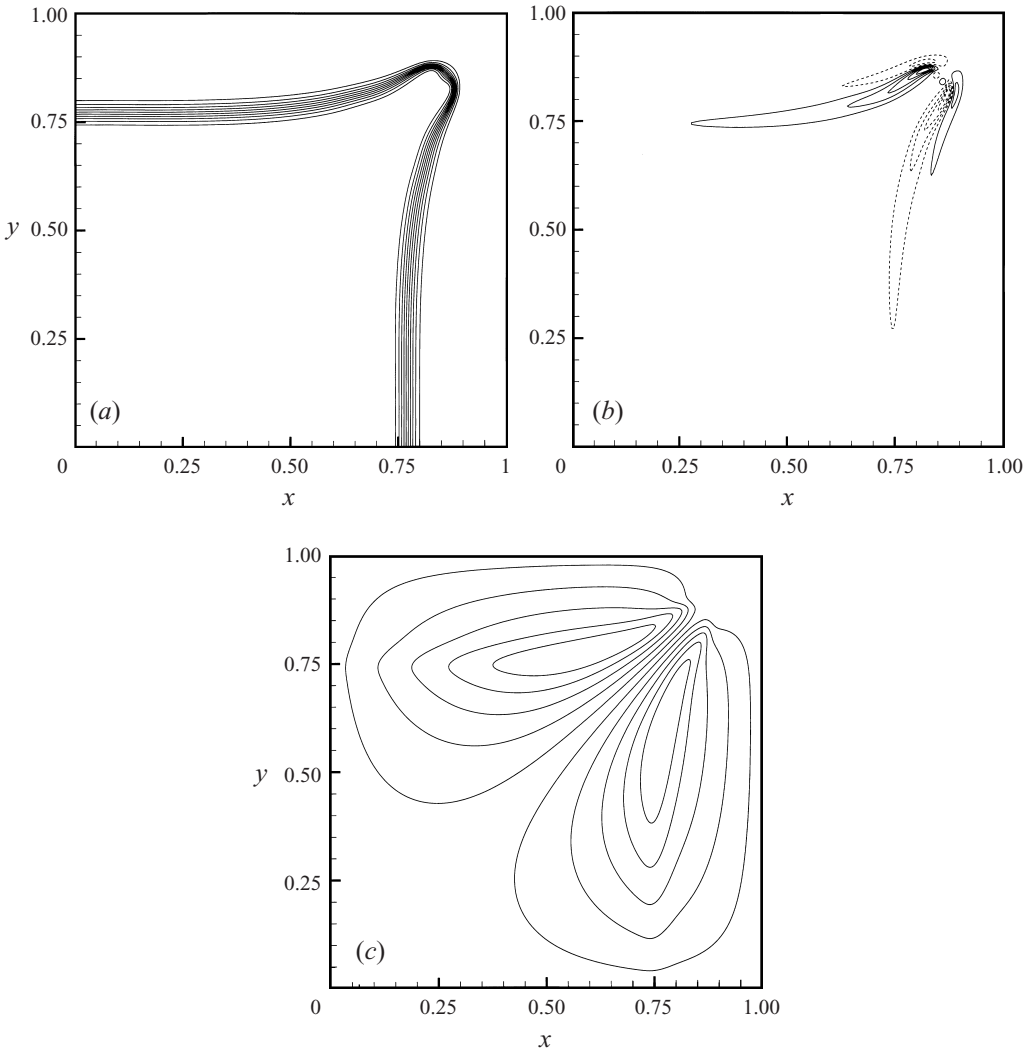

FIGURE 7. Contours of concentration (*a*), vorticity (*b*, negative values dashed), and perturbation streamfunction (*c*) for $Pe = 800$, $\alpha = 2.0$, $\mu_m = 3.0$, $c_m = 0.37$ at $t = 0.40$. All plots are scaled with the instantaneous maxima.

induce a backflow along the diagonal, thereby stabilizing the flow. It is important to realize that during the early stages of the flow, this phase is naturally determined by the differences between the quarter five-spot base flow and the purely radial base flow. If the base flow were strictly radial, the spatial phase could take arbitrary values.

3.2.1. *Breakthrough recovery*

Breakthrough recovery results, which were computed as described by Chen & Meiburg (1998*a*), are summarized in table 1 for the simulations discussed above. For the case of $Pe = 200$ and $c_m = 0.67$ only a lower estimate is provided, as the simulation became unstable shortly before breakthrough. The recovery values obtained for the present non-monotonic viscosity profiles should be compared with the non-diffusive potential unit mobility ratio flow considered by Morel-Seytoux (1965, 1966), as well

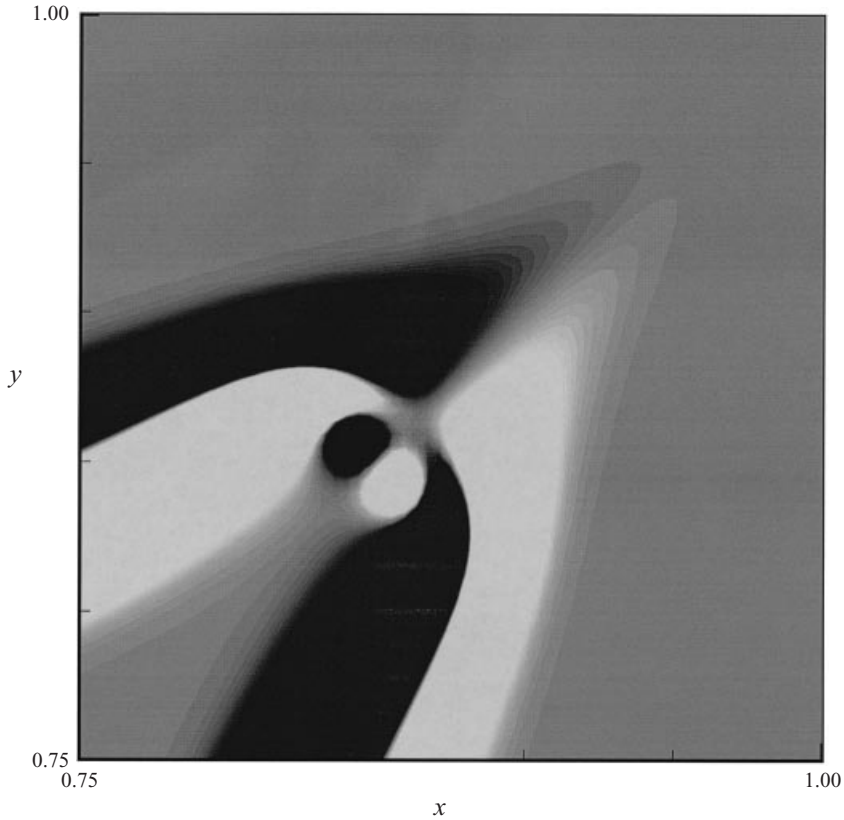

FIGURE 8. Vorticity (detail) for $Pe = 800$, $\alpha = 2.0$, $\mu_m = 3.0$ and $c_m = 0.37$ at $t = 0.40$. In order to emphasize the extent of the vortices, the plot is scaled with a value much lower than the instantaneous maximum. Dark indicate negative values, light areas positive values.

as with the results for exponential viscosity profiles for end-point viscosity contrasts of 2 and 0.5, respectively (C.-Y. Chen 1997, personal communication). The monotonic cases do not exhibit any fingering, whereas the non-monotonic cases at identical *Pe*-values do. This agrees with our earlier linear stability results, which showed non-monotonic viscosity profiles generally to have higher growth rates than their exponential counterparts with the same end-point viscosity ratio. Table 1 provides these growth rates predicted by linear theory.

Surprisingly, the tabulated results show that, even though the non-monotonic viscosity cases are characterized by higher instability growth rates, they nevertheless lead to significantly higher breakthrough recoveries than an exponential profile with an identical end-point viscosity ratio. In fact, the profile showing the most vigorous fingering also gives the highest recovery among the non-monotonic cases, which is even larger than that of the potential flow. As a further comparison, a non-monotonic case was simulated whose endpoint viscosities were identical to the maximum and displaced fluid viscosities, respectively, of the non-monotonic case with the highest recovery. This monotonic case showed an even better recovery. Viscous fingering generally has been viewed as the cause of early breakthrough, and consequently of reduced recovery. The above findings require us to re-evaluate the causal relationship between fingering and early breakthrough for non-monotonic viscosity–concentration relationships. For

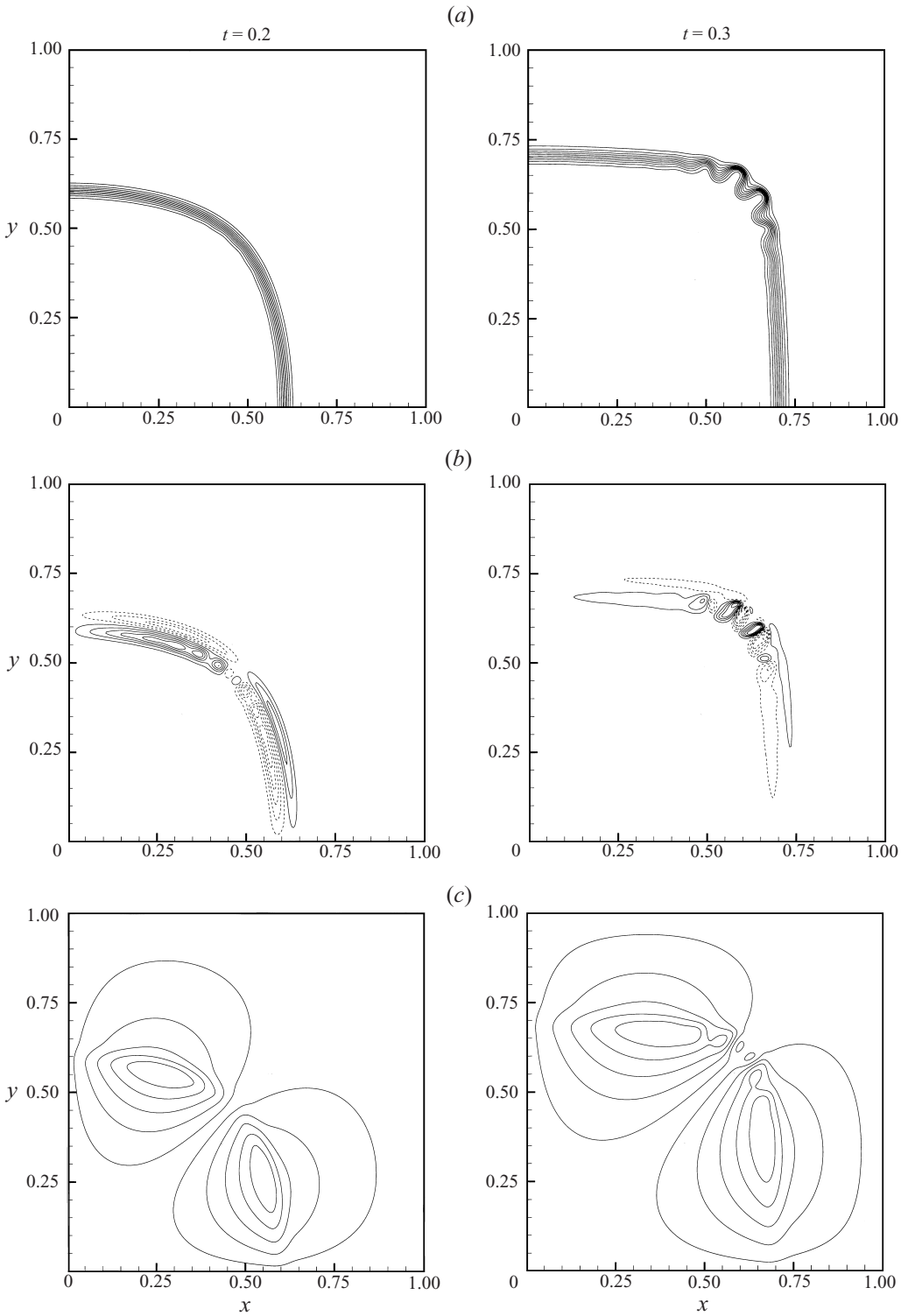

FIGURE 9. For caption see facing page.

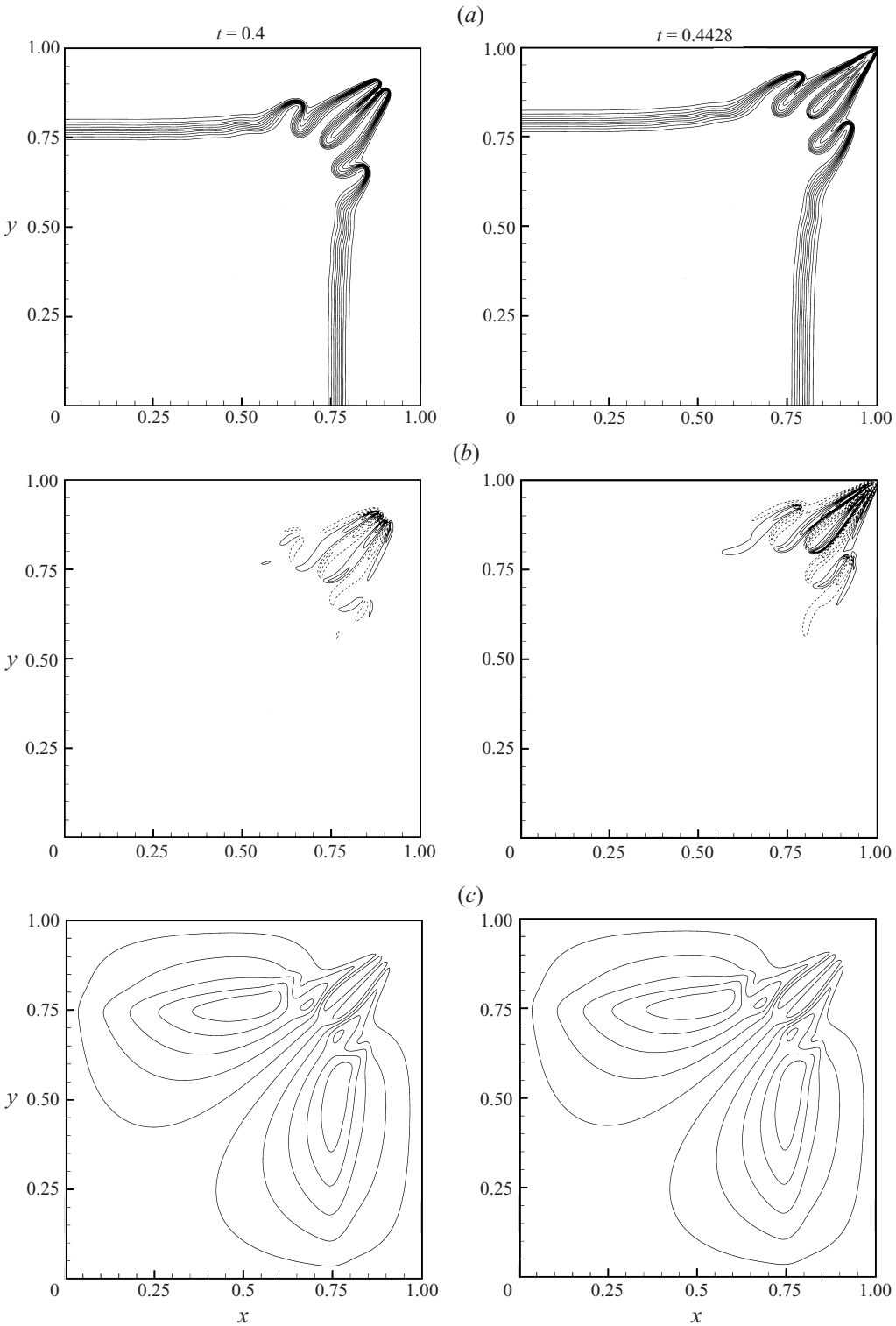

FIGURE 9. Time trace of the contours of concentration (*a*), vorticity (*b*, negative values dashed), and perturbation streamfunction (*c*) for $Pe = 800$, $\alpha = 2.0$, $\mu_m = 4.0$, $c_m = 0.25$. All plots are scaled with the instantaneous maxima. Breakthrough occurred at time t_b.

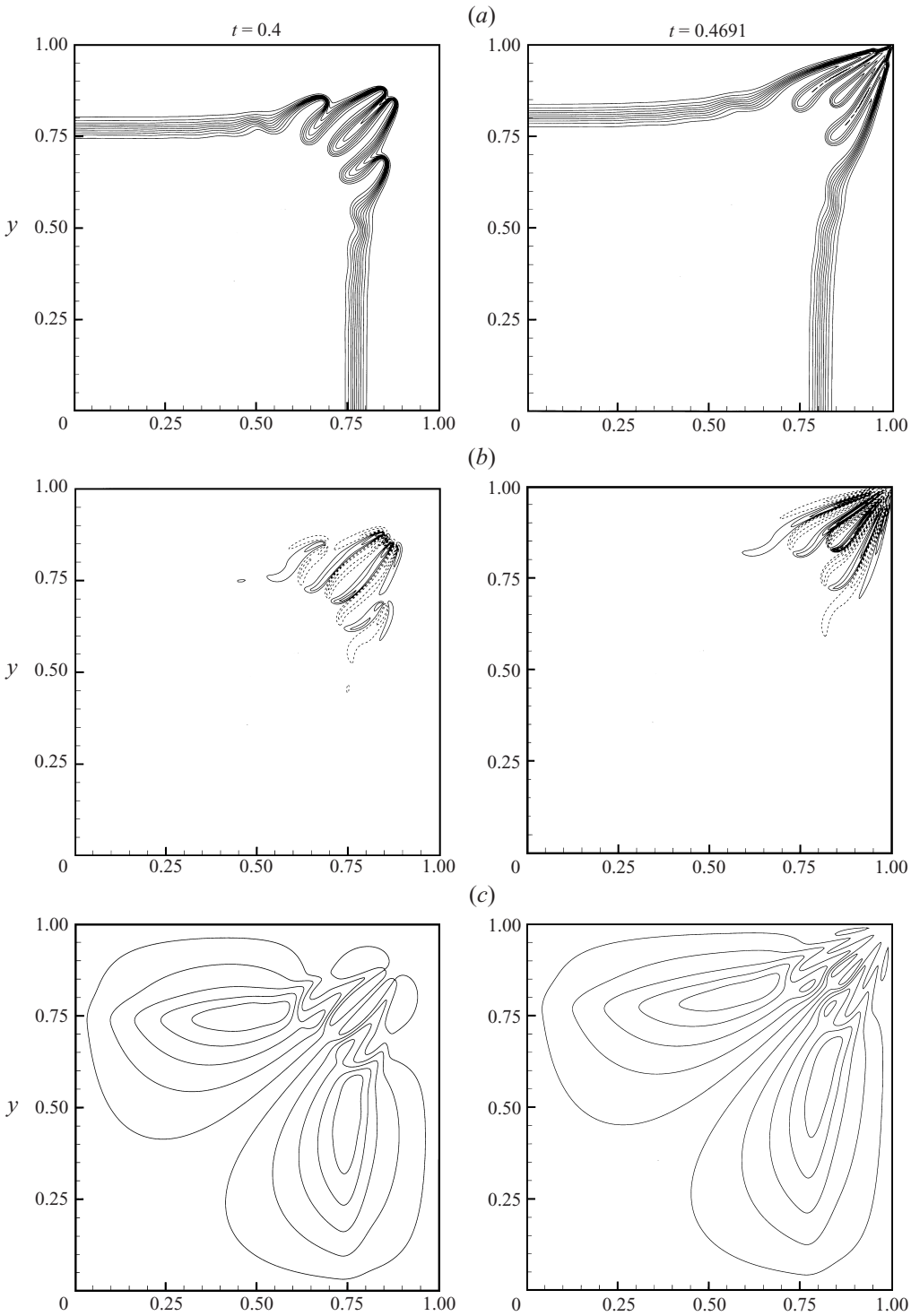

FIGURE 10. Time trace of the contours of concentration (*a*), vorticity (*b*, negative values dashed), and perturbation streamfunction (*c*) for $Pe = 800$, $\alpha = 2.0$, $\mu_m = 4.0$, $c_m = 0.37$. All plots are scaled with the instantaneous maxima. Breakthrough occurred at time t_b.

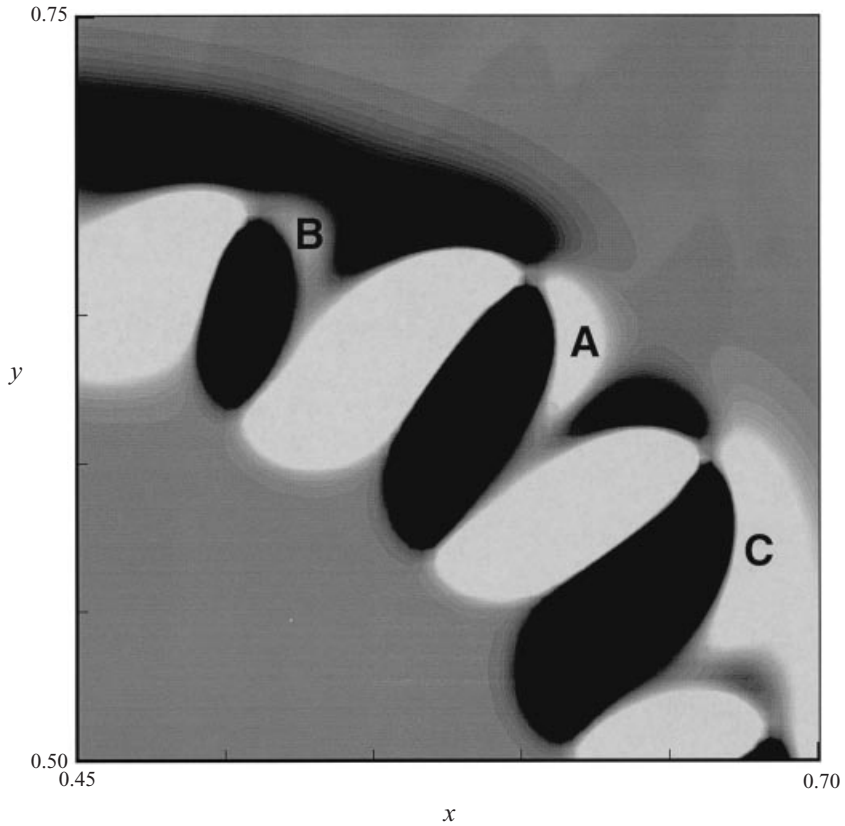

FIGURE 11. Vorticity (detail) for $Pe = 800$, $\alpha = 2.0$, $\mu_m = 4.0$ and $c_m = 0.37$ at $t = 0.30$. Dark areas indicate negative values, light areas indicate positive values. The details A–C are mentioned in the text.

these flows we find that fingering does not lead to early breakthrough, but rather the spatio-temporal development of the base flow becomes much more dominant. The concentration contours in figures 9 and 10 demonstrate the importance of the reverse fingering mechanism. Shortly before and even at breakthrough, we find the front to be smooth and almost without waves on the side of the displaced fluid. The fingering more or less completely takes place inside the displacing fluid. Breakthrough thus cannot be attributed to an outrunning finger, but rather to the base flow of the concentration front along the diagonal. Consequently, the quadrupole structure of the base flow generated by the non-monotonicity, i.e. the above-mentioned base-flow vorticity, can act to delay the breakthrough. This behaviour is most clearly visible in the displacement for $Pe = 800$, $\alpha = 2.0$, $\mu_m = 4.0$ and $c_m = 0.37$, which resulted in the highest efficiency. Figure 12 shows the perturbation streamfunction, the concentration field, and the vorticity field near the sink at $t = 0.45$, which is shortly before breakthrough. The concentration plot shows three viscous fingers of high-viscosity fluid penetrating into the displacing fluid, one along the diagonal and one on each side of it. The central finger already is nearly cut off from supply of high-viscosity fluid, and has begun to fade. The low-viscosity fluid is bypassing this finger on both sides. However, its breakthrough is delayed by two outer vortices, which have their origin in the base-flow quadrupole and still at this late time create

a counterflow along the diagonal. Simultaneously, they transport high-viscosity fluid from the sides to the sink. A comparison of the concentration contours in the time trace of figure 10 at $t = 0.40$ and at breakthrough demonstrates this behaviour.

To summarize our observations, we find that the outer pair of recirculating fluid regions, which originates in the base-flow quadrupole, represents the main influence on the breakthrough time, as it has the ability to impede the flow along the diagonal. The stronger these regions, and the longer they exist, the higher the displacement efficiency. The time over which these regions remain active strongly depends on the parameters of the non-monotonic viscosity profile. While there does not seem to be a straightforward way to predict recovery rates based on the growth rates obtained from linear stability theory, a few general observations can nevertheless been made. A lower viscosity maximum tends to weaken the recirculating fluid regions, as can be seen in figure 7, where for the reduced $\mu_m = 3.0$ the outer ones never become visible in the perturbation streamfunction plot. The sweep efficiency therefore is considerably lower than for the case of $\mu = 4.0$. The location of the viscosity maximum plays an interesting role as well. As pointed out in § 3.1, the larger zone of locally decreasing viscosity related to a higher c_m strengthens the outer recirculating fluid regions at later times, which defers breakthrough. This effect becomes more prominent when viscous fingering is present. At $Pe = 800$ and for $\mu_m = 4.0$, the two displacements with $c_m = 0.25$ and $c_m = 0.37$ result in efficiencies that differ by more than 4%. The perturbation streamfunction plots for these cases at $t = 0.40$ in figures 9(c) and 10(c) show that the deflection of low-viscosity fluid from the diagonal is much weaker for the lower c_m, as the counter-rotating fluid regions cannot act as effectively.

4. Summary and conclusions

The present investigation concerns the linear stability of miscible radial source flows, as well as the related nonlinear evolution of quarter five-spot displacements, in the presence of non-monotonic viscosity profiles. The viscosity–concentration relationships, first proposed by Manickam & Homsy (1993, 1994) are characterized by the three parameters of end-point viscosity contrast, maximum viscosity, and location of this maximum. The linear stability analysis demonstrates the existence of a critical value Pe_c for any combination of these parameters, above which the flow is unstable. Each of the three parameters has a significant influence on the growth rate, the wavenumber of the most dangerous mode, and the short-wave cutoff wavenumber. It is found that, for a given end-point viscosity contrast, an increase in the maximum viscosity generally leads to a more unstable flow, regardless of whether the overall viscosity ratio is favourable or not. This is in marked contrast to rectilinear displacements (Manickam & Homsy 1993), in which a higher maximum viscosity generally stabilizes flows with an unfavourable end-point viscosity ratio. The stability results are interpreted in detail, based on the eigensolutions of the linear problem. While the vorticity field always shows a quadrupole structure, the perturbation streamlines can organize in either one or two rings of counterrotating vortices. Depending on their strength, their location, and their interaction with the gradients in the viscosity profile, they can play either a destabilizing or a stabilizing role.

Quarter five-spot flows approximate radial source flows for small times, and very close agreement is observed between the growth rates predicted by linear theory for the latter, and those found in direct numerical simulations of the former. As for rectilinear flows, we observe reverse fingering to be the main feature of non-monotonic displacements. However, the base flow generated by the specific geometry

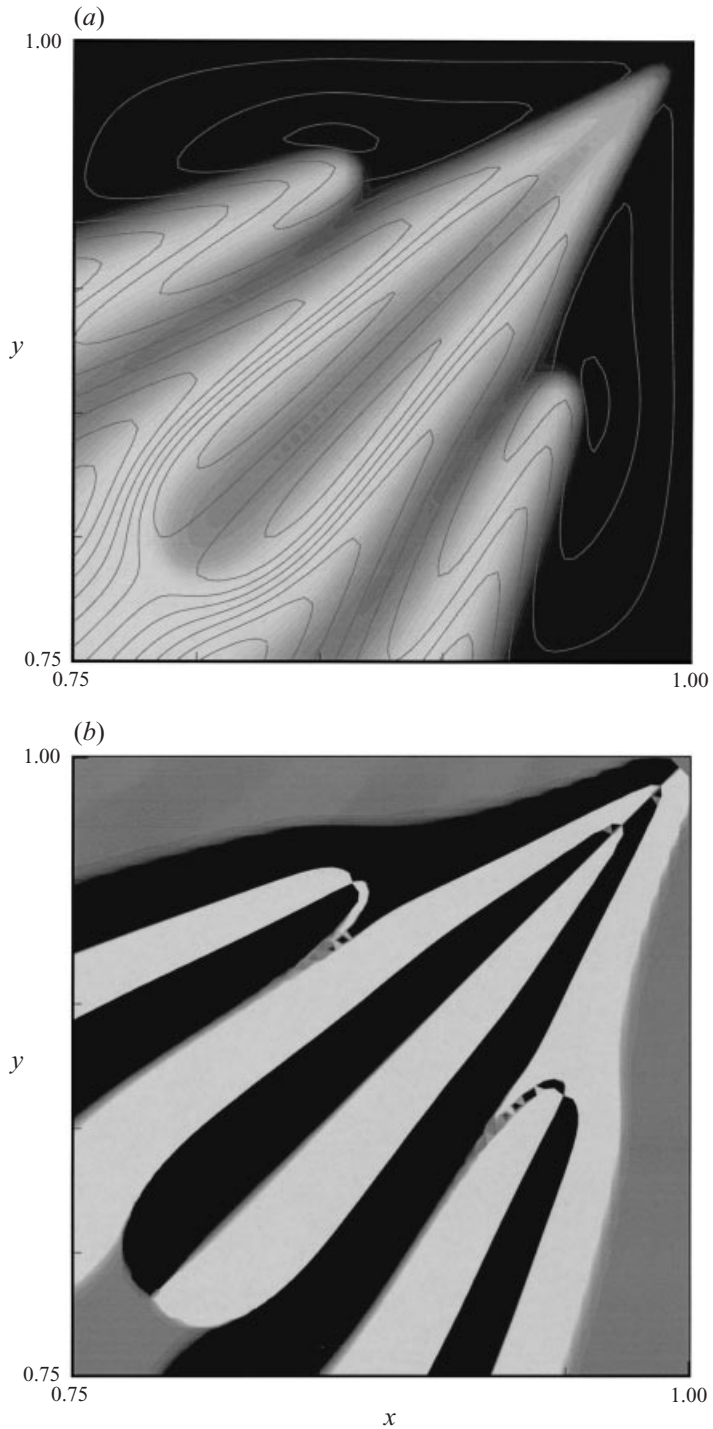

FIGURE 12. (*a*) Overlay of perturbation streamfunction and concentration (detail). Light areas correspond to high concencration of the displacing fluid. (*b*) Corresponding vorticity field, scaled with the maxima at $t = 0.10$. The plots show the displacement with $Pe = 800$, $\alpha = 2.0$, $\mu_m = 4.0$ and $c_m = 0.37$ at $t = 0.45$.

of the quarter five-spot arrangement turns out to play a crucial role as well. It is characterized by a quadrupole structure which enhances the flow along the diagonal on the side of the displacing fluid, while impeding it on the side of the displaced fluid. The interaction of reverse fingering and quadrupole-like base flow results in the remarkable consequence that viscosity profiles characterized by a strong instability and vigorous fingering at the same time may provide high breakthrough recoveries that can even exceed the efficiency of the unit mobility ratio flow. These findings suggest that the optimization of a displacement process should not focus exclusively on minimizing or eliminating the fingering instability, but rather on stimulating an optimal coupling between base flow and reverse fingering.

We thank Yanis Yortsos for helpful comments on an earlier version of the manuscript, as well as for bringing some of the references to our attention. Partial support by the donors of The Petroleum Research Fund (grant ACS-PRF # 33497-AC9), through a NATO Collaborative Research Grant, by the National Science Foundation in form of an equipment grant, and by the Chevron Petroleum Technology Company is gratefully acknowledged. The simulations were carried out at the San Diego Supercomputer Center, which is sponsored by NSF. We would also like to thank the Studienstiftung des deutschen Volkes (German National Merit Foundation) for supporting the visit of C. Pankiewitz at the University of Southern California by providing a travel grant.

REFERENCES

Bacri, J. C., Rakotomalala, N., Dalin, D. & Woumeni, R. 1992*a* Miscible viscous fingering: Experiments versus continuum approach. *Phys. Fluids* A **4**, 1611.

Bacri, J. C., Salin, D. & Yortsos, Y. 1992*b* Analyse lineaire de la stabilité de l'écoulement de fluides miscibles en milieux poreux. *C. R. Acad. Sci. Paris* **314**, 139.

Blunt, M. J. & Christie, M. A. 1991 Exact solutions for viscous fingering in two-phase, three-component flow. SPE-22613 *presented at the 66th Annual Technical Conference of the Society of Petroleum Engineers, Dallas, Texas, October 6–9, 1991.*

Brady, J. F. & Koch, D. L. 1988 In *Disorder and Mixing* (ed. E. Guyon, J.-P. Nadal & Y. Pomean) NATO ASI Series E. Kluwer.

Chen, C.-Y. & Meiburg, E. 1998*a* Miscible porous media displacements in the quarter five-spot configuration. Part 1. The homogeneous case. *J. Fluid Mech.* **371**, 233.

Chen, C.-Y. & Meiburg, E. 1998*b* Miscible porous media displacements in the quarter five-spot configuration. Part 2. Effect of heterogeneities. *J. Fluid Mech.* **371**, 269.

Chikhliwala, E. D., Huang, A. B. & Yortsos, Y. C. 1988 Numerical study of the linear stability of immiscible displacement processes in porous media. *Trans. Porous Media* **3**, 257.

Christie, M. A., Muggeridge, A. H., & Barley, J. J. 1991 3D simulation of viscous fingering and WAG schemes. *SPE* 21238, Presented at the 11th Symposium on Reservoir Simulation, Anaheim, CA.

Farouq Ali, S. M. 1970 *Oil Recovery by Steam Injection.* Producers Publ., Bradford.

Hickernell, F. J. & Yortsos, Y. C. 1986 Linear stability of miscible displacement processes in porous media in the absence of dispersions. *Stud. Appl. Maths* **74**, 93.

Latil, M. 1980 *Enhanced Oil Recovery.* Gulf.

Loggia, D., Salin, D. & Yortsos, Y. C. 1998 The effect of dispersion on the stability of non-monotonic mobility profiles in porous media. *Phys. Fluids* **10**, 747.

Manickam, O. & Homsy, G. M. 1993 Stability of miscible displacements in porous media with non-monotonic viscosity profiles. *Phys. Fluids* A **5**, 1356.

Manickam, O. & Homsy, G. M. 1994 Simulation of viscous fingering in miscible displacements with non-monotonic viscosity profiles. *Phys. Fluids* **6**, 95.

Meiburg, E. & Chen, C.-Y. 1998 High-accuracy implicit finite difference simulations of homogeneous and heterogeneous miscible porous media flows. (submitted). *SPE Res. Engng.*

Morel-Seytoux, H. J. 1965 Analytical-numerical method in waterflooding predictions. *Soc. Petrol. Engrs J.* September, 247.

Morel-Seytoux, H. J. 1966 Unit mobility ratio displacement calculations for pattern floods in homogeneous medium. *Soc. Petrol. Engrs J.* September, 217.

Pankiewitz, C. & Meiburg, E. 1998 Miscible porous media displacements in the quarter five-spot configuration. Part 3: Nonmonotonic viscosity profiles. *Center for Modeling and Simulation Rep.* CMS-98-1. University of Southern California.

Petitjeans, P., Chen, C.-Y., Meiburg, E. & Maxworthy, T. 1998 Miscible quarter five-spot displacements in a Hele-Shaw cell and the role of flow-induced dispersion. *Phys. Fluids* (submitted).

Rogerson, A. & Meiburg, E. 1993*a* Shear stabilization of miscible displacement processes in porous media. *Phys. Fluids* A **5**, 1344.

Rogerson, A. & Meiburg, E. 1993*b* Numerical simulation of miscible displacement processes in porous media flows under gravity. *Phys. Fluids* A **5**, 2644.

Tan, C. T. & Homsy, G. M. 1987 Stability of miscible displacements in porous media: Radial source flow. *Phys. Fluids* **30**, 1239.

Tan, C. T. & Homsy, G. M. 1988 Simulation of nonlinear viscous fingering in miscible displacement. *Phys. Fluids* **31**, 1330.

Yortsos, Y. C. 1987 Stability of displacement processes in porous media in radial flow geometries. *Phys. Fluids* **30**, 2928.

Yortsos, Y. C. & Zeybek, M. 1988 Dispersion driven instability in miscible displacement in porous media. *Phys. Fluids* **31**, 3511.

Zimmerman, W. B. & Homsy, G. M. 1991 Nonlinear viscous fingering in miscible displacement with anisotropic dispersion. *Phys. Fluids* A **3**, 1859.